Yerbilimleri, 2024, 45 (3), 185-207, 1491285

Hacettepe Üniversitesi Yerbilimleri Uygulama ve Araştırma Merkezi Bülteni (*Bulletin of the Earth Sciences Application and Research Centre of Hacettepe University*

YERBİLİMLERİ
Bulletin for Earth Sciences

ISSN: 2687- 2978

Preliminary Study of Scandium Enrichment in Çaldağ-Manisa Lateritic Ni-Co Deposit, Western Anatolia

Çaldağ-Manisa (Batı Anadolu) Lateritik Ni-Co Yatağındaki Skandiyum Zenginleşmesinin Ön Çalışması

NİLAY GÜLYÜZ [1,2*]

[1] Department of Geological Engineering, Van Yüzüncü Yıl University, Van, Türkiye

[2] Department of Neotectonics and Thermochronology, Institute of Rock Structure and Mechanics of the Czech Academy of Sciences, Prague, Czechia

Received *(geliş)*: 28 May (Mayıs) 2024 Accepted *(kabul):* 12 September (Eylül) 2024

ABSTRACT

Scandium is one of the most valuable critical metals, with high demand in applications ranging from biomedical research to electronics. Lateritic Ni-Co deposits are considered prime targets for scandium (Sc) exploration because Sc can be concentrated during weathering through residual and secondary enrichment, reaching up to 100 ppm and making it a potential by-product.

This study investigates the distribution of Sc in the unweathered parent rocks and various laterite zones within two distinct pits of the Çaldağ lateritic Ni-Co deposit in Western Anatolia. In the Hematite pit, the serpentinite protolith shows an average Sc content of 10.3 ppm, with significant enrichment in the middle-upper limonite zone, reaching up to ~66 ppm. Although this represents a sixfold increase compared to the serpentinite protolith, the maximum Sc concentrations (53.6–65.7 ppm) are relatively low compared to other nickel laterites with by-product Sc potential (~100 ppm). This lower concentration is attributed to the initial low Sc content of the serpentinized peridotite protolith and post-lateritization tectonic activity. Conversely, the South pit exhibits higher initial Sc content in the protolith (~13 ppm) but lower average Sc content (~6.4 ppm) in the limonite zone, likely due to post-lateritization dissolution of Sc-hosting minerals by alteration and secondary weathering processes within the highly deformed pit.

The findings suggest that while the Çaldağ deposit exhibits Sc concentrations up to ~66 ppm in the limonite zone, the potential for Sc as a by-product alongside Ni production is limited. Further detailed mineralogical and geochemical investigations are recommended to gain a deeper understanding of the mechanisms of Sc distribution in the Çaldağ deposit and other lateritic deposits in Türkiye.

Key words: Critical Metals, Lateritic Weathering, Nickel Laterites, Scandium, Serpentinite

ÖZ

Skandiyum, biyomedikal araştırmalardan elektroniğe kadar çeşitli uygulamalarda yüksek talep gören en değerli kritik metallerden biridir. Lateritik Ni-Co yatakları skandiyum (Sc) aramaları için başlıca hedefler olarak kabul edilir çünkü Sc bozuşma sırasında kalıntı ve ikincil zenginleştirme yoluyla konsantre olarak, 100 ppm'e kadar ulaşabilir ve potansiyel bir yan ürün haline gelebilir.

Bu çalışmada, Batı Anadolu'daki Çaldağ lateritik Ni-Co yatağının iki farklı ocağındaki bozuşmamış ana kayaçlarda ve çeşitli laterit zonlarında Sc dağılımı incelenmiştir. Hematit ocağında, serpantinit protolit ortalama 10,3 ppm Sc içeriği gösterirken, orta-üst limonit zonunda ~66 ppm'e kadar ulaşan önemli bir zenginleşme görülmektedir. Bu serpantinit protolitine kıyasla altı katlık bir artışı temsil etmesine rağmen, maksimum Sc konsantrasyonları (53,6-65,7 ppm) yan ürün Sc potansiyeline sahip diğer nikel lateritlere (~100 ppm) kıyasla nispeten düşüktür. Bu düşük konsantrasyon, serpantinleşmiş peridotit protolitin başlangıçtaki düşük Sc içeriğine ve lateritleşme sonrası tektonik aktiviteye bağlanmaktadır. Buna karşılık, Güney ocağında protolitte daha yüksek başlangıç Sc içeriği (~13 ppm), ancak limonit zonunda daha düşük ortalama Sc içeriği (~6,4 ppm) sergilenmektedir; bunun olası nedeni Sc barındıran minerallerin yüksek oranda deforme olmuş ocak içindeki alterasyon ve ikincil bozuşma süreçleri tarafından lateritleşme sonrası çözünmesidir.

Bulgular, Çaldağ yatağının limonit zonlarında ~66 ppm'e kadar Sc konsantrasyonları sergilemesine rağmen, Ni üretiminin yanı sıra bir yan ürün olarak Sc potansiyelinin sınırlı olduğunu göstermektedir. Çaldağ yatağındaki ve Türkiye'deki diğer lateritik yataklardaki Sc dağılım mekanizmalarının daha iyi anlaşılabilmesi için daha detaylı mineralojik ve jeokimyasal araştırmalar yapılması önerilmektedir.

Anahtar Kelimeler: *Kritik Metaller, Lateritik Bozuşma, Nikel Lateritler, Skandiyum, Serpantinit*

https://doi.org/10.17824/yerbilimleri.1491285

*Corresponding Author/Sorumlu Yazar: nilaygulyuz@yyu.edu.tr

INTRODUCTION

Scandium, which is widely used in modern technology, renewable energy, and the aerospace and automotive industries, was included in the critical raw materials list revised by the European Union Commission in 2017 (European Union Commission, 2017) because of the growing market need for it (Emsley, 2014; Gambogi, 2018; Polyak, 2018; Ulrich et al., 2019). In light of the recent global potential for critical metals, including scandium, lateritic Ni-Co deposits formed on ultramafic rocks (such as those in Cuba, the Dominican Republic, Australia, and New Caledonia) with Sc concentrations ~100 ppm, which are suitable for the extraction of scandium as a by-product, have been identified as important targets for exploration to reduce the supply risk of Sc.

In nature, scandium is not found alone; rather, it is found in combination with other minerals (Maulana et al., 2016). As a compatible element, Sc is found in higher proportions in mafic and ultramafic rocks than in other igneous rocks. In ultramafic rocks, which are the source rock of the lateritic Ni deposits, Sc takes place in the structure of hornblende, olivine, and biotite, but mainly clinopyroxene minerals (Leeman and Scheidegger, 1977; Aiglsperger et al., 2016; Maulana et al., 2016; Samson and Chassé, 2016; Ulrich et al., 2019). Scandium, which can be enriched in an amount that can be exploited as a by-product as a result of weathering, is found in almost every zone of a lateritic profile and reaches the highest amounts in the limonite zone, which usually represents the upper levels of a lateritic profile (Audet, 2009; Jaireth et al., 2014; Aiglsperger et al., 2016; Maulana et al., 2016; Rangott et al., 2016; Chassé et al., 2017; Ulrich et al., 2019). Whole-rock analyses of the laterites and the strong positive correlation of iron with Sc indicate that scandium is concentrated in the ferric iron (Fe^{3+})-containing end products of lateritization, goethite, and hematite minerals. According to the detailed mineral chemistry analysis studies, 80% of the Sc concentration in Eastern Australian laterites is found in goethite, while 20% of it is detected

in hematite (Chassé et al., 2017). In New Caledonian laterites, on the other hand, the highest Sc values are observed in the goethite mineral (average 82.7 ppm, the highest 136 ppm), while an average of 47.5 ppm Sc is detected in hematite, up to 76.6 ppm (Ulrich et al., 2019). Thus, in lateritic Ni deposits, the goethite mineral can be identified as the primary Sc host.

Thus far, a few studies (Chassé et al., 2017; Munoz et al., 2017; Ulrich et al., 2019; Teitler et al., 2019) have investigated the genesis of scandium enrichment in lateritic deposits. Scandium, which is found in ultramafic rocks, especially in pyroxene minerals, dissolves during lateritic weathering, causing the water circulating in the regolith below the water table to be enriched in Sc. Under the acidic pH condition (4-6; Fandeur et al., 2009), and high water and humidity activity, goethite minerals precipitate, and Sc^{3+} (Brookins, 1988), following the Fe^{3+} form in nature, is adsorbed on goethite (Chassé et al., 2017). In dry periods, however, with higher temperatures, decreased water activity, and near-neutral pH conditions (6–8; Gleeson et al., 2003; Marsh et al., 2013), as hematite develops and crystallizes, a portion of the adsorbed scandium (about 50%) becomes part of the crystal structure. The size difference between the six-fold coordinated Sc^{3+} and Fe^{3+}, however, limits this mechanism, although such size differences will not affect the adsorption capacity of goethite under near-neutral pH conditions (Chassé et al., 2017; Ulrich et al., 2019). Although it is claimed that the decreasing Sc concentration from the yellow limonite zone (goethite-dominant) to the red limonite zone (hematite-dominant) and iron cap (ferricrete) in a lateritic profile is connected to the Sc content of the goethite itself (Teitler et al., 2019), the Sc enrichment mechanism described above supports that the Sc amounts observed in the upper levels of a lateritic profile and decreasing from the yellow limonite zone to the iron cap (ferricrete) are controlled by the increased amount of hematite compared to goethite (Ulrich et al., 2019).

As a result, lateritic Ni deposits, in general, can show Sc enrichment up to about 10 times that of the unweathered parent rock. However, the duration of the weathering process and tectonic stability are key factors controlling the Sc enrichment in these deposits. Consequently, in lateritic Ni deposits, three processes work together to produce exceptionally high Sc concentrations: (1) abnormally high Sc concentration in the unweathered parent rock; (2) prolonged weathering in a stable tectonic environment; and (3) lateritic conditions that provide trap of Sc by iron oxides during weathering (Chassé et al., 2017).

In Türkiye, ultramafic rocks with the potential to form lateritic Ni±Co deposits are represented by generally E-W trending ophiolitic outcrops along with the İzmir-Ankara-Erzincan suture belt associated with the Alpine-Himalayan orogenic belt (Okay and Tüysüz, 1999). Although the ophiolitic rocks in Türkiye are common, there are a limited number of lateritic Ni±Co deposits developed on them (Figure 1) under tropical to subtropical climatic conditions from Cretaceous to Miocene, and only some of them are economically exploited: Çaldağ (Manisa), Gördes (Manisa), Muratdağı (Uşak), Karaçam (Eskişehir), and Sarıçimen (Van) (Elitok and Tavlan, 2019). There are some studies on the geology, geochemistry, and mineralogy of these deposits (Çolakoğlu, 2009; Thorne et al., 2009; Tavlan et al., 2011;

Helvacı et al., 2018; Serin, 2020; Kılıç et al., 2021). However, limited research have been done to investigate the scandium content of these deposits.

In this study, the first information on the distribution and concentration of Scandium (Sc) along the lateritic weathering profiles of one of the most important lateritic deposits, Çaldağ (Manisa) lateritic Ni-Co deposit, is provided, and the scandium enrichment potential of the deposit is evaluated in light of available literature data. Additionally, the study has implications for the scandium enrichment potential of lateritic Ni(-Co) deposits in Türkiye.

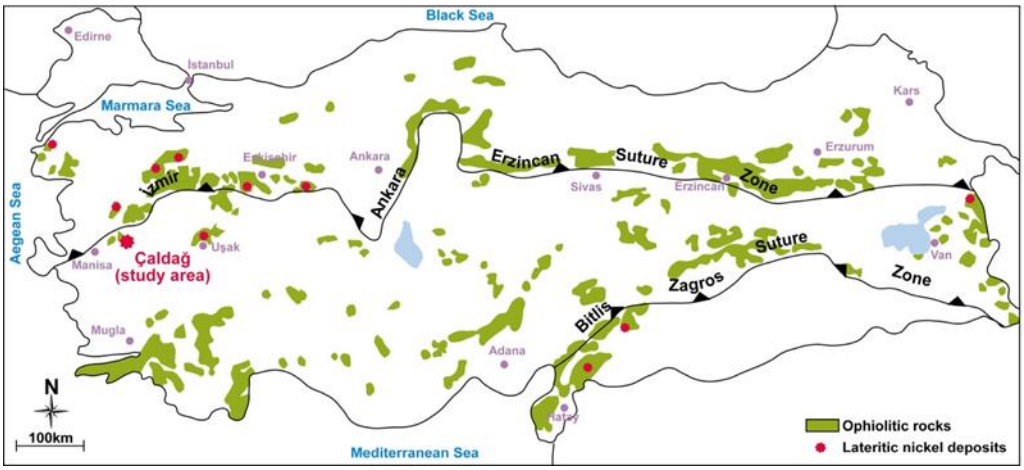

Figure 1. Distribution of ophiolitic rocks and lateritic nickel deposits in Türkiye (modified from Elitok and Tavlan, 2019).

Şekil 1. *Türkiye'de ofiyolitik kayaçların ve lateritik nikel yataklarının dağılımı (Elitok ve Tavlan, 2019'dan değiştirilmiştir).*

GEOLOGICAL SETTING AND THE FORMATION OF THE ÇALDAĞ DEPOSIT

The Çaldağ lateritic Ni-Co deposit is located approximately 25 km north of Turgutlu (Manisa) and about 70 km east of İzmir in Western Anatolia (Figure 2a). It covers an area of around 9 km² and has a reserve of 33.3 Mt with 1.14% Ni and 0.07% Co (Thorne et al., 2009). The deposit is situated between the İzmir-Ankara-Erzincan suture zone and the Menderes Massif, and lies within the Bornova Flysch Zone (BFZ) that thrusts over the Paleozoic-aged metamorphic basement rocks of the Menderes Massif in the northwest of the Anatolide-Tauride Block (Okay and Siyako, 1993; Figure 2a). The BFZ was formed on the Mesozoic continental margin of the Anatolide-Tauride Block in an ocean that evolved during the late Cretaceous-early Paleocene period (Okay and Siyako, 1993; Okay et al., 1996). It consists of Upper Cretaceous-Lower Paleocene greywacke and shale alternations, and includes Mesozoic-aged limestone olistoliths. This zone is associated with Cretaceous oceanic accretionary prism products, which widely outcrop in the region (Okay and Tüysüz, 1999). In the Çaldağ deposit area, the BFZ is represented by ultrabasic (harzburgite-dunite), serpentinized ultrabasic, and spilitic volcanic rocks, along with a matrix consisting of sandstone, conglomerate, claystone, limestone, radiolarite, chert, and dolomitic limestones (Tavlan et al., 2011). Approximately 50 km

northeast of the deposit, ophiolites associated with the BFZ are overlain by the late Ypresian (late Early Eocene) Başlamış Formation. Although this formation consists of basal conglomerates derived from ophiolite overlain by sandstone, marl, and limestones, fragments derived from laterites are not observed, suggesting that the outcropping, erosion, and active weathering of the ophiolite were limited to the pre-Early Eocene period (Akdeniz, 1980; Önoğlu, 2000). That means that lateritization in the deposit began in the late Paleocene–early Eocene (Tavlan et al., 2011; Thorne et al., 2012).

The N-S-directed extensional neotectonic regime that has been dominant in Western Anatolia since the latest Oligocene (e.g. Bozkurt, 2001; Gülyüz et al., 2024a) has led to the formation of horsts and deep grabens that cut through the Menderes Massif and associated continental basins (e.g., Koçyiğit et al., 1999; Bozkurt, 2001; Bozkurt and Sözbilir, 2004; Figure 2a). The Çaldağ deposit is located within the northernmost Gediz Graben, and the Gediz detachment fault, responsible for the extension in the north of the graben, was dated at 20-18 Ma (amphibole Ar/Ar; Lips et al., 2001). It is likely that during this extensional phase, ultramafics associated with the BFZ in the Çaldağ area, which may have been covered by post-Paleocene units, were exposed to weathering and subsequent lateritization. However, the overlay of the deposit by the Develi Formation in the late Miocene (Messinian) suggests the late Miocene period as the upper limit of the lateritization process (Kaya et al., 2004).

An evaluation of the climatic conditions in the Çaldağ region under the optimum climatic conditions shows that the most suitable climate for the lateritization of the Çaldağ ophiolite prevailed in the Middle Eocene (Thorne et al., 2012). Additionally, Helvacı et al. (2013) propose two separate periods of lateritization in the Çaldağ deposit, based on detailed petrography and SEM studies, and structural analysis from field studies: (1) Late Paleocene-Middle Eocene, and (2) Oligocene.

Weathering profiles in the Çaldağ deposit are observed in three different pits: (1) Hematite pit, (2) North pit, and (3) South pit (Figure 2b). While these profiles are generally similar, they present local differences in texture, morphology, and chemical and mineralogical composition. According to Thorne et al. (2009), the main ore zone, the limonite (oxide) zone, is found above the variably serpentinized ultramafics (peridotites) in the profiles of the deposit, and it is overlain by a redder hematite zone and covered by Eocene-aged lacustrine limestones in the south and a siliceous level in the north. The limited development of Ni-silicates and the lack of a sizable saprolite zone indicate that the deposit is an oxide-type lateritic Ni deposit (Thorne et al., 2009).

The main ore mineral is goethite, found within the limonite zone of the deposit, while asbolane, takovite, serpentine, limonite, nontronite, and montmorillonite have elevated Ni and Co values. Quartz, chalcedony, chromite, and hematite are gangue minerals observed within non-nickeliferous zones (Thorne et al., 2009; Helvacı et al., 2018).

SAMPLING AND METHODOLOGY

Sampling Strategy

In the Çaldağ deposit, detailed mapping and macroscopic examination of lateritic weathering profiles were conducted across various pits to delineate each laterite zone precisely and facilitate targeted sample collection for studying the distribution of scandium (Sc).

The lateritic profiles at the Hematite and South pits, largely preserved from erosion, were chosen for comprehensive sampling from the protolith to the ferricrete zone. Sample

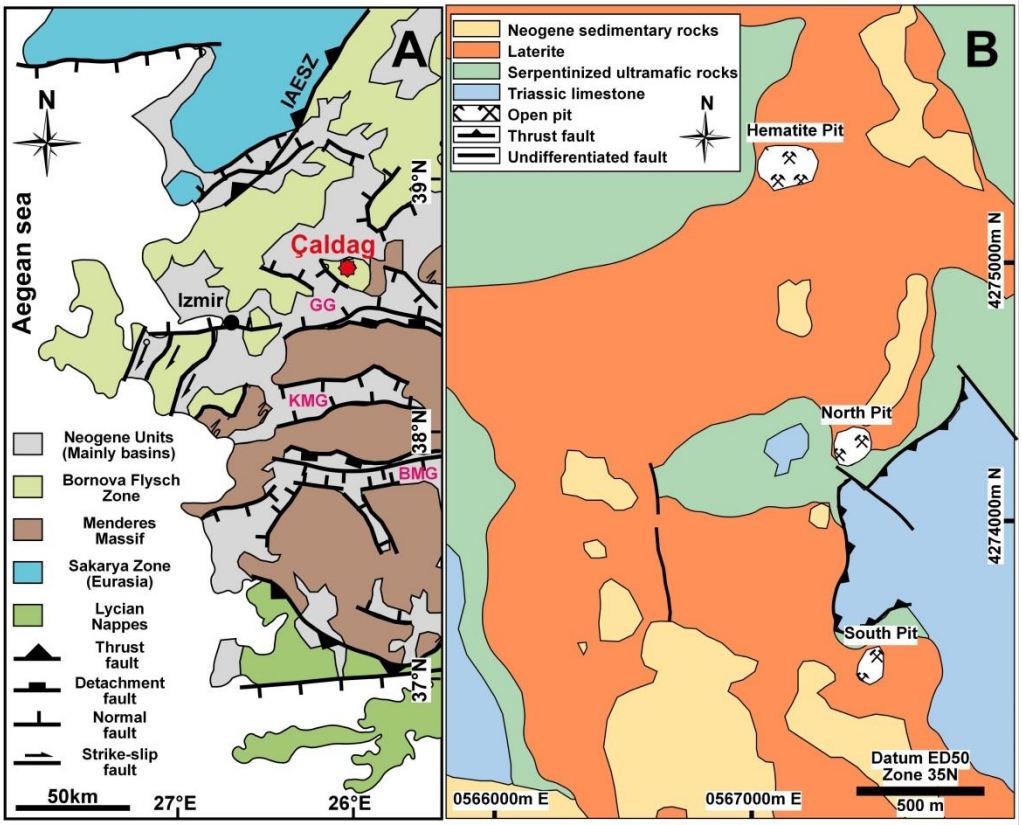

Figure 2. (A) Simplified geological map of Western Anatolia with the location of the Çaldağ deposit (IAESZ: İzmir-Ankara-Erzincan Suture Zone; GG: Gediz Graben; KMG: Küçük Menderes Graben; BMG: Büyük Menderes Graben) (modified from Tavlan et al. 2011 and Gülyüz et al. 2024b). **(B)** Simplified geological map of the Çaldağ deposit and surrounding area with the locations of the three pits (modified from Helvacı et al. 2018 and Gülyüz et al. 2024b).

Şekil 2. (A) *Çaldağ yatağının konumunu gösteren basitleştirilmiş Batı Anadolu jeoloji haritası (IAESZ: İzmir-Ankara-Erzincan Kenet Kuşağı; GG: Gediz Grabeni; KMG: Küçük Menderes Grabeni; BMG: Büyük Menderes Grabeni) (Tavlan vd. 2011 ve Gülyüz vd. 2024b'den değiştirilmiştir).* ***(B)*** *Çaldağ yatağı ve çevresinin basitleştirilmiş jeolojik haritası ile üç ocağının konumları (Helvacı vd. 2018 ve Gülyüz vd. 2024b'den değiştirilmiştir).*

collection was systematically performed along the open pit walls where the profiles are exposed.

Specifically, at the Hematite pit, two extensive lateritic profiles were studied, one along the eastern wall and another on the north-western wall (Figure 3a). Grab sampling was conducted from the three profiles. The eastern profile, approximately 40 meters thick, yielded 17 samples: 3 from the serpentinite protolith, 8 from altered serpentinite, 6 from the limonite zone, and 6 from the ferricrete zone. The north-western profile, about 48 meters thick, provided 19 samples: 3 from the serpentinite protolith, 3 from altered serpentinite, 6 from the limonite zone, and 7 from the ferricrete zone.

In the South pit, a shorter and less deformed section at the base of a roughly 12-meter thick profile (Figure 3b) was sampled, resulting in 2 samples from the serpentinite protolith and 3 from the limonite zone. The hematite zone of

the pit could not be sampled because it was not accessible.

Sampling could not be conducted in the North pit due to the discontinuity of the laterite zones, which were heavily disrupted by faulting, movement, landslides, and overturning. In total, 47 samples were collected from the Çaldağ deposit: 8 from the unweathered parent rock serpentinite and 39 from various laterite zones across the different profiles. This systematic approach ensures a thorough investigation of the lateritic profiles and their respective zones, providing crucial insights into the Sc distribution within the deposit.

Figure 3. General view of the Çaldağ deposit: **(A)** Hematite pit with the two mapped lateritic profiles. **(B)** South pit with the mapped laterite profile (taken from Gülyüz et al. 2024b).

Şekil 3. *Çaldağ yatağının genel görünümü:* ***(A)*** *Haritalanmış iki lateritik profil ile Hematit ocağı.* ***(B)*** *Haritalanmış laterit profili ile Güney ocağı (Gülyüz vd. 2024b'den alınmıştır).*

Geochemical Analyses

Geochemical analyses were carried out at the geochemistry laboratories of the General Directorate of Mineral Research and Exploration in Ankara, Türkiye. In this context, the weathered ultramafic rock and laterite samples were analyzed for concentrations of scandium (Sc) and other trace elements such as cobalt (Co), nickel (Ni), vanadium (V), and chromium (Cr) using inductively coupled plasma mass spectroscopy (ICP-MS). Additionally, the concentrations of major oxides

(Al_2O_3, CaO, Fe_2O_3, K_2O, MgO, MnO, Na_2O, P_2O_5, SiO_2, and TiO_2), and the percentage of loss on ignition (LOI) were measured using X-ray fluorescence (XRF) spectroscopy.

RESULTS

General Characteristics of Lateritic Profiles

Various laterite zones and the exposed protolith were mapped macroscopically along two lateritic profiles from the Hematite pit and one shorter lateritic profile from the South pit (Figure 3). Schematics of these lateritic profiles, and sample locations for geochemical analyses are presented in Figure 4.

Hematite pit

The lateritic profiles in the Hematite pit, exposed on both the eastern and north-western walls, exhibit some textural, mineralogical, and morphological variations, although the lateritic zones are generally consistent across the pit (Figure 4). The protolith is characterized by whitish, light green-brown serpentinite, overlaid by dark yellow-brownish altered serpentinite. Above this lies a partly siliceous limonite zone enriched with goethite, and the uppermost level features a partly brecciated silica-rich iron cap (ferricrete).

On the eastern wall, the exposed protolith of serpentinized peridotite features whitish, light green stockwork calcite veins (Figure 5a). Upwards in the section, within the dark yellow-light brown altered serpentinite, brown irregular goethite-rich veins appear (Figure 5b), increasing in density near the transition to the limonite zone. This transition is gradual, with massive colloform goethites becoming dominant. At the base of the limonite zone, approximately 3 meters thick, the texture of altered serpentinite is locally preserved, presenting a fine-grained, dark yellowish-brown structure with continuous massive colloform goethite veins (Figure 5c). Ascending through the limonite zone, the residual serpentinite disappears, the goethite veins become more irregular and sparse, and the limonite zone transitions into a partially silicified state approaching the ferricrete zone, which has a fragmented blocky structure. The limonite zone culminates in completely silicified, dark yellow-dark brown massive goethite displaying a gossan-like boxwork structure (Figure 5d). The overlying ferricrete zone, dark reddish-brown and silica-rich, exhibits a brecciated structure with fragments cemented by dark brownish siliceous goethite (Figure 5e). Residual chromite crystals (Figure 5f) are visible in the polygonal opal, quartz, and chalcedony fragments of the poorly sorted breccias. The total thickness of this lateritic profile is approximately 40 meters (Gülyüz et al., 2024b).

On the north-western wall, the protolith of fractured serpentinized peridotite with whitish calcite and iron oxide veins transitions into dark yellow-light green-brown altered serpentinite featuring common irregular calcite and magnesite veins accompanied by thin iron oxide stockwork veins (Figure 6a-b). The limonite zone here begins with some residual serpentinite and common irregular goethite veins (Figure 6c), evolving into banded goethite in its upper levels, with a tilt of approximately 60–80° to the northeast. Near the brecciated ferricrete zone at the upper level of the limonite zone, the weathering within the zone increases, and silicified, generally massive but sometimes continuous dark brown-black vein-like goethite (Figure 6d) is found instead of the banded goethite in the lower zone. The contact between this upper level of the limonite zone and the ferricrete zone is transitional rather than sharp, and in this transition zone, silicified goethite and limonite (Figure 6e) with gossan texture are found in places. When the ferricrete zone is reached, a very dark red-brown-black colored weathered blocky and brecciated structure is observed.

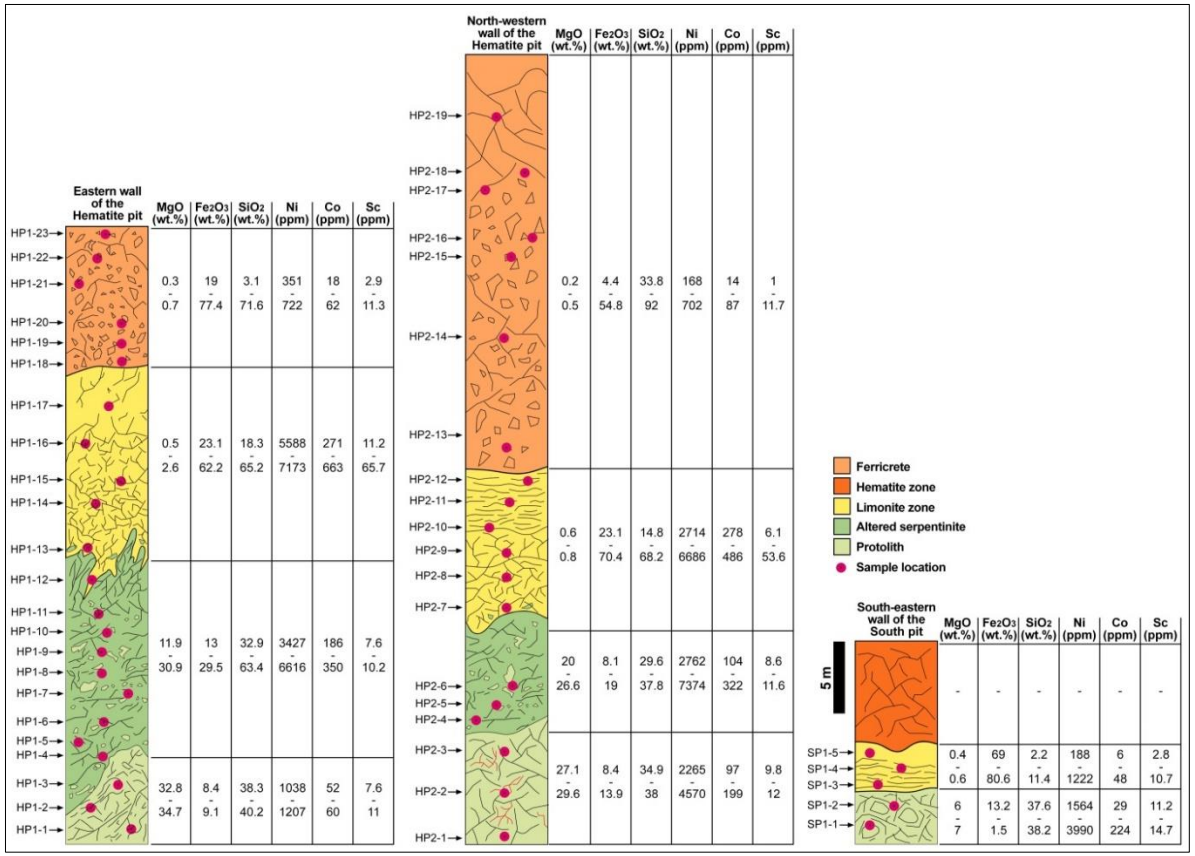

Figure 4. Schematics of the lateritic profiles in the Çaldağ deposit showing location of samples and characteristic assay results (modified from Gülyüz et al. 2024b).

Şekil 4. *Çaldağ yatağındaki lateritik profillerin örneklerin yerlerini ve karakteristik analiz sonuçlarını gösteren şemas (Gülyüz vd. 2024b'den değiştirilmiştir).*

Angular chalcedony and silica containing isolated chromite crystals form the parts of the breccias, while massive siliceous goethite is observed as cementing the breccias and as continuous veins cutting the zone (Figure 6f). This lateritic profile measures approximately 48 meters in thickness (Gülyüz et al., 2024b).

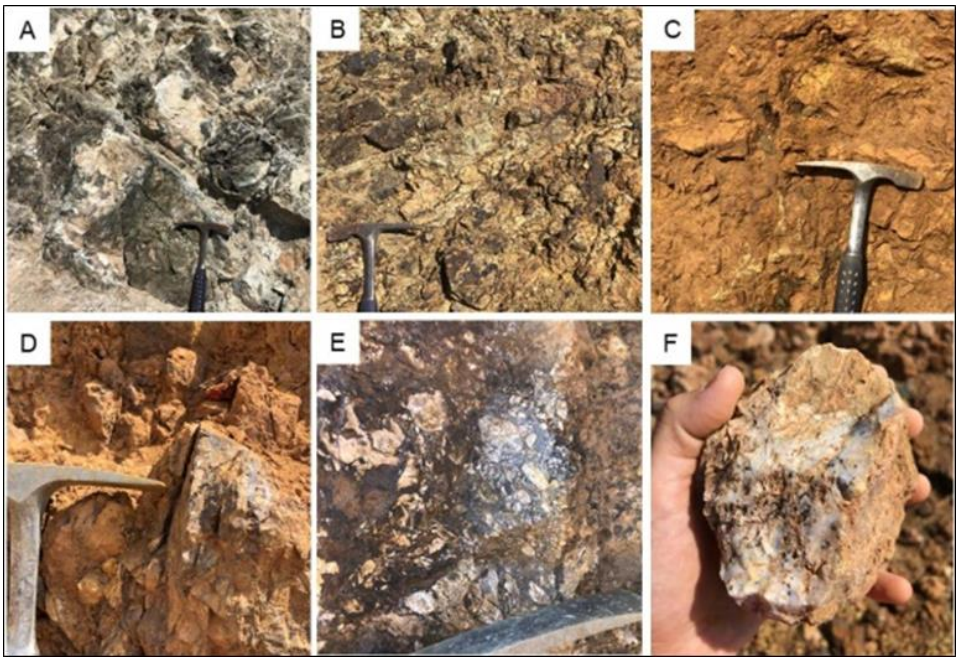

Figure 5. (A) Serpentinite protolith with stockwork calcite veins. **(B)** Altered serpentinite with irregular goethite-rich veins. **(C)** Lower levels of limonite zone with stockwork goethite veins and relict serpentinite. **(D)** Upper levels of the limonite zone with silicified massive goethite. **(E)** Ferricrete zone with brecciated silica cemented by massive goethite. **(F)** Relict chromite crystals within the chalcedony from the ferricrete zone (B-C-D-E-F taken from Gülyüz et al. 2024b).

Şekil 5. (A) *Stokvörk kalsit damarları içeren serpantinit protoliti.* ***(B)*** *Düzensiz götit zengini damarlara sahip altere serpantinit.* ***(C)*** *Stokvörk götit damarları ve kalıntı serpantinit içeren limonit zonunun alt seviyeleri.* ***(D)*** *Silisleşmiş masif götit içeren limonit zonunun üst seviyeleri.* ***(E)*** *Masif götit ile çimentolanmış breşleşmiş silika içeren ferricrete zonu.* ***(F)*** *Ferricrete zonundaki kalsedon içinde kalıntı kromit kristalleri (B-C-D-E-F Gülyüz vd.2024b'den alınmıştır).*

South pit

The lateritic profile in the South pit, dipping about 40° to the southwest, consists of a serpentinite protolith at the base, followed by a limonite zone and an allochthonous hematite zone at the top (Figure 7a). This profile exhibits significant morphological changes due to post-mineral juxtaposition, overturning, and faulting. The protolith below is light-dark green, partially weathered oxidized serpentinite (Figure 7b) containing a black peridotite core with residual olivine and pyroxene crystals. The transition from the partly weathered serpentinite to the limonite zone is marked by dark yellow-brown goethite with localized limonite bands. Ascending through the limonite zone, banded goethite gives way to weathered-comminuted massive goethite with calcite infill. The overlying dark red-brown hematite zone, completely allochthonous, is characterized by brecciated structures and calcite cementing siliceous goethite-limonite blocks with

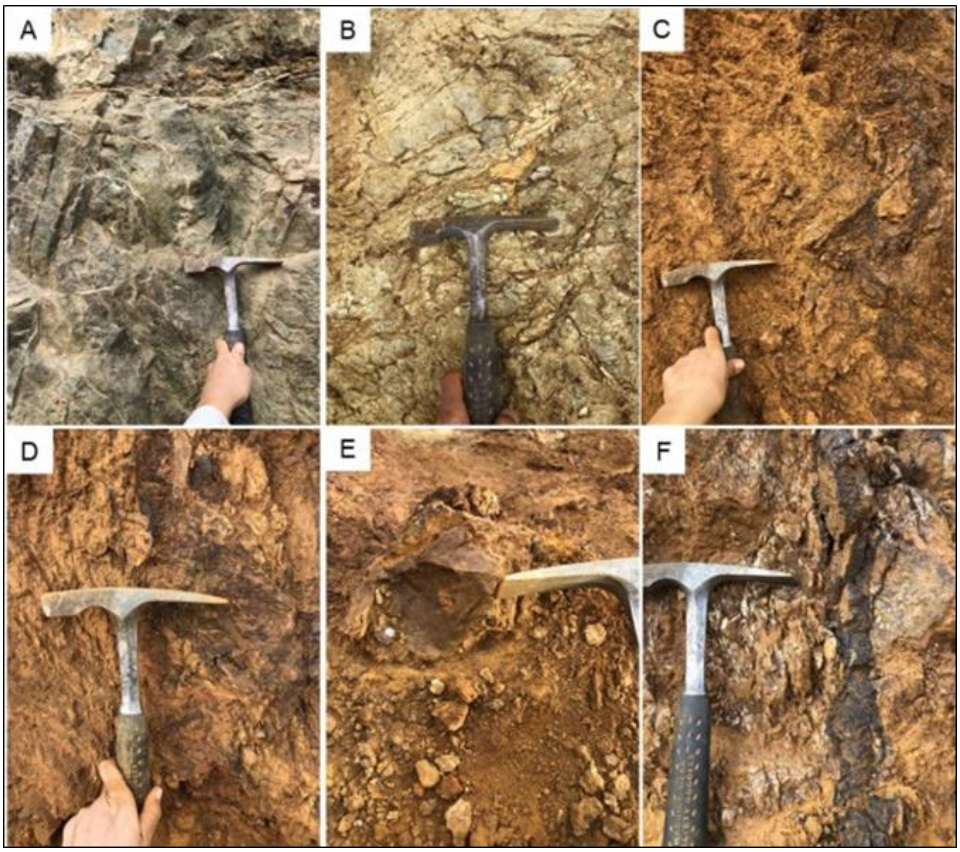

Figure 6. (A) Fractured altered serpentinite dominated by stockwork calcite and magnesite veins. **(B)** Altered serpentinite rich in iron-oxide veinlets. **(C)** Lower levels of limonite zone with occasional relict serpentinite and irregular goethite veins. **(D)** Middle to upper levels of limonite zone with silicified massive goethite and occasionally vein goethite. **(E)** Upper levels of the limonite zone with siliceous goethite and limonite in gossan texture. **(F)** Ferricrete zone with irregular goethite veins and brecciated silica cemented by massive silicieous goethite (B-C-E-F taken from Gülyüz et al. 2024b).

Şekil 6. (A) *Stokvörk kalsit ve manyezit damarlarının hakim olduğu kırıklı altere serpantinit. (**B**) Demir oksit damarları bakımından zengin altere serpantinit. **(C)** Ara sıra kalıntı serpantinit ve düzensiz götit damarları içeren limonit zonunun alt seviyeleri. **(D)** Silisleşmiş masif götit ve yer yer damar götit içeren limonit zonunun orta ve üst seviyeleri. **(E)** Gossan dokusunda silisli götit ve limonit içeren limonit zonunun üst seviyeleri. **(F)** Masif silisli götit ile çimentolanmış düzensiz götit damarları ve breşleşmiş silika içeren ferricrete zonu (B-C-E-F Gülyüz vd.2024b'den alınmıştır).*

intersecting veins (Figure 7a). The thickness of this lateritic profile, excluding the protolith, is estimated to be around 12 meters (Gülyüz et al., 2024b).

Geochemistry of Lateritic Profiles

Composition of major oxides (Al_2O_3, CaO, Fe_2O_3, K_2O, MgO, MnO, Na_2O, P_2O_5, SiO_2, and TiO_2) and loss on ignition (LOI), transition

Table 1. Content of major oxides, transition metals (Ni, Co, Cr, V), critical metal Sc, and loss on ignition (LOI) in samples of the Çaldağ deposit (n = 47).

Tablo 1. *Çaldağ yatağı örneklerinde (n = 47) majör oksitler, geçiş metalleri (Ni, Co, Cr, V), kritik metal Sc ve tutuşma kaybı (LOI) içeriği.*

Profile	Sample ID	LOI* (%)	Al_2O_3 (%)	CaO (%)	Fe_2O_3 (%)	K_2O (%)	MgO (%)	MnO (%)	Na_2O (%)	P_2O_5 (%)	SiO_2 (%)	TiO_2 (%)	Cr (ppm)	Co (ppm)	Ni (ppm)	V (ppm)	Sc (ppm)	Zone
Hematite pit profile 1 (Eastern wall)	HP1-1	14.1	0.4	1.8	9.1	<0.1	34.5	0.1	<0.1	<0.1	39.2	<0.1	225	60.00	1207	8.0	10.5	Serpentinite protolith
	HP1-2	15.0	0.1	4.6	8.4	<0.1	32.8	<0.1	<0.1	<0.1	38.3	<0.1	12	57.00	1132	<5	7.6	
	HP1-3	13.9	0.4	0.9	9.1	<0.1	34.7	0.1	<0.1	<0.1	40.2	<0.1	244	52.00	1038	9.0	11.0	
	HP1-4	13.5	0.4	0.2	14.0	<0.1	30.9	0.1	<0.1	<0.1	39.2	<0.1	337	188.00	4383	10.0	10.2	Altered serpentinite
	HP1-5	14.0	1.3	1.4	16.9	<0.1	28.5	0.3	<0.1	<0.1	36.2	<0.1	153	188.00	3427	9.0	8.8	
	HP1-6	16.2	0.3	7.1	13.0	<0.1	26.8	0.2	<0.1	<0.1	35.0	<0.1	128	186.00	3867	7.0	10.2	
	HP1-7	12.8	1.4	0.4	25.4	<0.1	25.1	0.3	<0.1	<0.1	32.9	<0.1	66	289.00	5088	10.0	9.5	
	HP1-8	9.7	<0.1	<0.1	26.6	<0.1	17.3	0.2	<0.1	<0.1	44.0	<0.1	23	259.00	5145	<5	7.6	
	HP1-9	10.0	0.1	0.2	29.5	<0.1	13.6	0.2	<0.1	<0.1	44.3	<0.1	61	257.00	5375	5.0	8.7	
	HP1-10	13.0	0.2	0.2	24.6	<0.1	24.4	0.3	<0.1	<0.1	35.0	<0.1	142	350.00	6616	7.0	8.9	
	HP1-11	7.6	<0.1	0.1	14.4	<0.1	11.9	0.2	<0.1	<0.1	63.4	<0.1	241	233.00	5203	6.0	7.8	
	HP1-12	6.2	0.1	0.1	23.1	<0.1	2.6	0.2	<0.1	<0.1	65.2	<0.1	831	389.00	5672	14.0	12.2	Limonite zone
	HP1-13	7.6	0.3	0.3	36.3	<0.1	1.1	0.6	<0.1	<0.1	51.6	<0.1	466	705.00	6252	<5	11.2	
	HP1-14	10.2	0.5	0.3	50.4	<0.1	0.6	0.6	<0.1	<0.1	34.7	<0.1	416	626.00	5737	<5	30.5	
	HP1-15	14.4	6.7	0.4	50.5	<0.1	0.9	0.6	<0.1	<0.1	23.2	<0.1	1481	663.00	7173	5.0	65.7	
	HP1-16	11.1	2.1	0.2	45.4	<0.1	0.5	0.2	<0.1	<0.1	37.6	<0.1	762	271.00	6196	9.0	63.6	
	HP1-17	13.2	1.8	0.2	62.2	<0.1	0.6	0.3	<0.1	<0.1	18.3	<0.1	807	330.00	5588	18.0	19.9	
	HP1-18	11.0	1.2	0.1	49.0	<0.1	0.3	0.1	<0.1	<0.1	32.1	<0.1	8240	55.00	722	107.0	7.0	Ferricrete
	HP1-19	12.7	0.5	0.1	77.4	<0.1	0.3	<0.1	<0.1	<0.1	3.1	<0.1	6148	24.00	595	56.0	11.3	
	HP1-20	12.0	0.4	0.1	74.5	<0.1	0.3	<0.1	<0.1	<0.1	9.4	<0.1	3747	18.00	369	24.0	3.0	

	HP1-21	5.8	1.6	0.2	19.0	0.10	0.5	<0.1	<0.1	<0.1	71.6	<0.1	1531	28.00	351	6.0	4.7	
	HP1-22	4.0	1.7	0.1	21.8	0.10	0.7	<0.1	<0.1	<0.1	67.6	<0.1	1673	26.00	365	16.0	2.9	
	HP1-23	12.9	0.6	0.1	75.3	<0.1	0.4	0.1	<0.1	0.10	6.4	<0.1	3925	62.00	693	124.0	7.4	
Hematite pit profile 2 (Northwestern wall)	HP2-1	16.8	0.4	1.7	13.9	<0.1	27.1	0.2	<0.1	<0.1	38.0	<0.1	286	199.00	4570	12.0	12.0	Serpentinite protolith
	HP2-2	16.2	0.3	3.4	12.6	<0.1	28.4	0.1	<0.1	<0.1	37.6	<0.1	268	177.00	3949	10.0	9.8	
	HP2-3	19.5	0.2	6.2	8.4	<0.1	29.6	0.2	<0.1	<0.1	34.9	<0.1	276	97.00	2265	11.0	10.7	
	HP2-4	13.5	0.2	0.6	19.0	<0.1	26.6	0.4	<0.1	<0.1	37.3	<0.1	194	322.00	7374	8.0	11.6	Altered serpentinite
	HP2-5	14.8	0.3	3.9	15.9	<0.1	25.4	0.3	<0.1	<0.1	37.8	<0.1	262	168.00	4710	9.0	10.1	
	HP2-6	22.3	0.2	18.6	8.1	<0.1	20.0	0.1	<0.1	<0.1	29.6	<0.1	108	104.00	2762	6.0	8.6	
	HP2-7	5.2	0.1	0.1	25.2	<0.1	0.6	0.2	<0.1	<0.1	66.3	<0.1	160	278.00	6686	<5	6.1	Limonite zone
	HP2-8	5.4	0.2	0.1	25.6	<0.1	0.6	0.3	<0.1	<0.1	65.5	<0.1	164	408.00	6396	<5	7.6	
	HP2-9	4.8	0.2	0.1	23.1	<0.1	0.6	0.2	<0.1	<0.1	68.2	<0.1	134	379.00	6247	<5	7.5	
	HP2-10	5.3	0.7	0.1	26.9	<0.1	0.8	0.1	<0.1	<0.1	63.6	<0.1	368	230.00	4798	8.0	21.0	
	HP2-11	8.4	2.7	0.1	41.9	<0.1	0.7	0.4	<0.1	<0.1	40.8	<0.1	2604	486.00	5302	7.0	53.6	
	HP2-12	10.6	0.8	0.1	70.4	<0.1	0.6	0.5	<0.1	<0.1	14.8	<0.1	932	356.00	2714	16.0	12.1	
	HP2-13	2.7	0.3	<0.1	12.3	<0.1	0.3	<0.1	<0.1	<0.1	83.3	<0.1	1319	21.00	521	38.0	3.9	Ferricrete
	HP2-14	6.2	0.4	0.1	21.0	<0.1	0.4	<0.1	<0.1	<0.1	70.5	<0.1	810	44.00	598	21.0	6.2	
	HP2-15	1.6	0.3	<0.1	4.4	<0.1	0.5	<0.1	<0.1	<0.1	91.5	<0.1	617	19.00	334	12.0	1.4	
	HP2-16	1.7	0.2	<0.1	4.8	<0.1	0.2	<0.1	<0.1	<0.1	92.0	<0.1	654	14.00	168	12.0	1.0	
	HP2-17	10.0	0.8	0.1	51.0	<0.1	0.2	<0.1	<0.1	<0.1	36.3	<0.1	1232	87.00	702	37.0	11.7	
	HP2-18	8.4	0.4	0.1	54.8	<0.1	0.3	<0.1	<0.1	<0.1	33.8	<0.1	1251	47.00	424	11.0	5.7	
	HP2-19	3.7	0.5	0.1	19.9	<0.1	0.5	<0.1	<0.1	<0.1	74.0	<0.1	721	23.00	200	78.0	1.9	
South pit profile	SP1-1	7.4	12.6	18.6	13.2	<0.1	7.0	0.2	0.10	0.60	37.6	2.10	107	29.00	1654	43.0	11.2	Protolith
	SP1-2	8.4	14.0	13.2	15.0	<0.1	6.0	0.5	0.10	0.60	38.2	2.20	470	224.00	3990	45.0	14.7	
	SP1-3	11.9	2.0	0.3	69.0	<0.1	0.6	0.1	<0.1	0.10	11.4	0.10	3923	48.00	952	38.0	10.7	Limonite zone
	SP1-4	12.5	0.8	0.2	76.5	<0.1	0.4	0.1	<0.1	<0.1	5.6	<0.1	1532	38.00	1222	31.0	5.6	
	SP1-5	11.7	0.8	0.2	80.6	<0.1	0.6	<0.1	<0.1	<0.1	2.2	<0.1	1078	6.00	188	31.0	2.8	

Figure 7. (A) A general view of the laterite zones exposed in the south pit. **(B)** Sharp contact between the serpentinite protolith and limonite zone at the base of the profile (taken from Gülyüz et al. 2024b).

Şekil 7. (A) *Güney ocağında yüzeyleyen laterit zonlarının genel görünümü.* ***(B)*** *Profilin tabanında serpantinit protolit ile limonit zonu arasındaki keskin dokanak (Gülyüz vd. 2024b'den alınmıştır).*

metals (Ni, Co, Cr, V), and critical metal Sc in samples collected from the Çaldağ deposit (n=47) is presented in Table 1.

Hematite pit

The geochemical data from the first lateritic weathering profile on the eastern wall of the Hematite pit and the second profile on the NW wall reveal distinct variations in the concentrations of SiO_2, Fe_2O_3, MgO, Ni, Co, Cr, V, and Sc along the profiles.

Silicon Dioxide (SiO_2): SiO_2 concentrations range from 3.1% to 92%, varying inversely along the weathering profiles. Typically, SiO_2 content is between 30-70%, with maximum concentrations in the ferricrete zone at the top of the profiles.

Iron Oxide (Fe_2O_3): Fe_2O_3 concentrations range from 4.4% to 77.4%. They are relatively low in the serpentinite protolith (8.4-13.9%) and altered serpentinite zone (8.1-29%) and show no consistent trend along the profiles, with uneven distribution between 15-60%. Fe_2O_3 concentrations vary between 23.1% to 70.4% within the limonite zone.

Magnesium Oxide (MgO): MgO values in the serpentinite protolith and altered serpentinite range from 11.9-34.7%, averaging 25.74%. MgO content decreases significantly in the transition to the limonite zone, falling below 1% and continuing to decrease towards the top.

Nickel (Ni): In the first profile, Ni concentration in the serpentinite protolith varies between 1038 ppm and 1207 ppm, increasing towards the ferricrete zone. Ni averages 4888 ppm in altered serpentinite and 6103 ppm in the limonite zone but decreases to an average of 515.83 ppm at the top. In the second profile, Ni values are higher, averaging 3594.67 ppm in the serpentinite protolith and 4948.67 ppm in altered serpentinite, reaching 5357.17 ppm in the limonite zone, and dropping to 168-702 ppm in the ferricrete zone.

Cobalt (Co): Co concentrations follow a similar trend to Ni. In the first profile, Co values range from 52-60 ppm in the protolith, increasing to an average of 243.75 ppm in altered serpentinite and 497.33 ppm in the limonite zone, and then decreasing to 18-62 ppm in the ferricrete zone. In the second profile, Co

averages 177.83 ppm in the protolith and altered serpentinite, 356.17 ppm in the limonite zone, and 11-78 ppm in the ferricrete zone.

Chromium (Cr): Cr concentrations are irregular in the protolith and altered serpentinite but increase significantly in the limonite zone. In the first profile, Cr ranges from 12-337 ppm in serpentinites, reaching 466-1738 ppm in the limonite zone and 1531-8240 ppm in the ferricrete zone. In the second profile, Cr values range from 108-368 ppm up to the ferricrete zone, with higher values detected in the limonite zone (932 ppm and 2604 ppm) and a gradual increase in the ferricrete zone (617-1319 ppm).

Vanadium (V): V concentrations are irregular in both profiles, ranging from <5 ppm to 18 ppm. Maximum V values (78 ppm and 124 ppm) are observed in the ferricrete zone, with mean concentrations of 55.5 ppm and 29.86 ppm in the ferricrete zones of the two profiles.

Scandium (Sc): Sc concentrations are similar in serpentinite protolith and altered serpentinite, ranging from 7.6 ppm to 12 ppm. The average Sc content in serpentinite protolith is 10.27 ppm, decreasing to 9.27 ppm in altered serpentinite. Sc values increase in the limonite zone, peaking at 53.6-65.7 ppm in the middle of the zone and decreasing towards the top. In the first profile, Sc values in the limonite zone vary between 11.2 ppm and 65.7 ppm, averaging 33.85 ppm. In the second profile, Sc values range from 6.1 ppm to 53.6 ppm, averaging 17.98 ppm. In the ferricrete zone, Sc values decrease to 1-11.7 ppm, with averages of 6.05 ppm in the first profile and 4.54 ppm in the second profile.

In summary, the average Sc content of 9.7 ppm in protolith serpentinite at the bottom of the first profile of the Hematite pit reaches 33.85 ppm by enriching approximately 3.5 times in the limonite zone. With the enrichment of scandium, which has 10.83 ppm in the serpentinite protolith at the base of the second alteration profile, its average value reaches 17.98 ppm in the limonite zone.

South pit

Due to interruptions caused by post-lateritization events such as transport and faulting, continuous sampling from bottom to top was not feasible in the weathering profile of the South pit. Therefore, geochemical analyses were conducted on five samples from the serpentinite protolith and the limonite zone, which maintains continuity at the base of the profile on the tilted pit wall.

Silicon Dioxide (SiO_2): In the intact serpentinite protolith, SiO_2 concentrations range from 37.6% to 38.3%. SiO2 concentrations decrease abruptly due to leaching in the transition to the limonite zone, averaging 6.4%, with a maximum of 11.4% and a minimum of 2.2%.

Iron Oxide (Fe_2O_3): Fe_2O_3 content in the serpentinite protolith ranges from 13.2% to 15%. In the limonite zone, Fe_2O_3 content increases sharply, ranging from 69% to 80.6%, with an average of 75.37%.

Magnesium Oxide (MgO): MgO concentrations in the protolith serpentinite are 6% and 7%. These concentrations decrease abruptly in the limonite zone, presenting values of 0.4% and 0.6%.

Nickel (Ni): Ni concentrations are higher in the protolith and lower in the limonite zone. Ni content in the protolith is 1654 ppm and 3990 ppm. In the limonite zone, Ni averages 787.33 ppm, with values of 188 ppm, 952 ppm, and 1222 ppm.

Cobalt (Co): Co concentration in the South pit profile is unevenly distributed, ranging from 6 ppm to 224 ppm.

Chromium (Cr): Cr concentrations in the serpentinite protolith are 107 ppm and 470 ppm. In the limonite zone, Cr shows a significant increase, with values of 1078 ppm, 1532 ppm, and 3923 ppm, averaging 2177.67 ppm.

Scandium (Sc): The Sc distribution in the South pit profile differs from that in the Hematite pit. Sc concentrations in the protolith are 11.2 ppm and 14.7 ppm, while lower Sc content is detected in the limonite zone at 2.8 ppm, 5.6 ppm, and 10.7 ppm values.

DISCUSSION

Scandium Enrichment Potential of the Çaldağ Lateritic Ni-Co Deposit

Lateritic Ni deposits can show Sc enrichment by 4-10 times of the amount of Sc in the unweathered bedrock (Chassé et al., 2017; 2019; 2020; Wang et al., 2021). However, few recent studies on scandium enrichment in a lateritic Ni-Co deposit have demonstrated the existence of many factors controlling Sc enrichment in these deposits. The duration of the weathering process and tectonic stability are major factors controlling the Sc enrichment in these deposits. Furthermore, a combination of three factors leads to very high Sc concentrations in lateritic Ni deposits: (1) abnormally high Sc concentration in unweathered bedrock, which is the first-order control on the Sc enrichment (Wang et al., 2021), (2) prolonged weathering in a stable tectonic environment, and (3) lateritic conditions that cause trapping of Sc into iron oxides during weathering (Chassé et al., 2017). Clinopyroxene and orthopyroxene, which are the main rock minerals forming the protolith in lateritic Ni-Co deposits, are the main sources of Sc, while hornblende, olivine and biotite are other minerals having high Sc content. Scandium, which can be enriched by lateritization, is found in almost every zone of a lateritic profile and generally reaches the highest amounts in the limonite zone. However, the enriched Sc is concentrated within final weathering products containing ferric iron (Fe^{3+}), goethite and hematite minerals (Chassé et al., 2019; Ulrich et al., 2019). Although detailed mineral chemistry studies in related deposits showing Sc enrichment reveal that Sc has a complex preferential affinity for goethite or hematite that can be modified by a variety of parameters, including specific surface area, physicochemical circumstances during crystallization, and distinct precursor minerals (Chassé et al., 2019; 2020; Qin et al., 2020; Wang et al., 2021), goethite is the most important Sc major mineral in lateritic Ni deposits.

In this context, during the evaluation of the scandium potential of the Çaldağ deposit according to the geochemical data of the samples collected from different lateritic zones, (1) the type of ultramafic protolith outcropping in the Hematite pit and South pit, (2) the presence of goethite and hematite minerals in different zones of the different lateritic profiles of the deposit and (3) tectonic stability of the deposit during- and after the lateritization were considered.

Additional geochemical analyses were conducted to investigate the Sc potential of the Çaldağ deposit. Considering the geochemical data obtained along the two lateritic profiles in the Hematite pit; (1) the dramatic decrease in MgO concentration during the transition from protolith to limonite and (2) the general decrease in Ni values over the limonite zone (Figure 4) indicate leaching events observed in an in-situ laterite (e.g., Marsh. et al., 2013). In addition, high Cr and V concentrations observed in the ferricrete zone (Table 1), the uppermost zone of laterite in both laterite profiles, are because of the presence of these elements in primary chromites (Traore et al., 2008), which are more resistant to weathering

compared to other minerals, and in pyroxene. It is thought that Cr and V values (Table 1) are the result of continuous enrichment in the upper levels of laterite due to the integration of goethite and/or hematite with the dissolution of pyroxene (Fandeur et al., 2009; Oze et al., 2004).

Hematite pit

When the scandium (Sc) values in the Hematite pit are examined, the scandium (Sc) concentrations in the serpentinite protolith and altered serpentinite are similar, and the average Sc content in the serpentinite protolith is 10.27 ppm, while this value is 9.27 ppm in the altered serpentinite. Although Sc values increase after passing into the limonite zone, they reach a maximum level (53.6-65.7 ppm) in the middle of the limonite zone and present a decreasing trend towards the upper levels of the zone. While the Sc values obtained from the limonite zone of the first profile vary between 11.2 ppm and 65.7 ppm, their average is 33.85 ppm. The Sc values obtained from the limonite zone of the second profile are lower than those of the first profile, offering values ranging from 6.1 ppm to 53.6 ppm with a mean of 17.98 ppm. The average Sc content in the limonite zone of both profiles of the Hematite pit was calculated as 25.92 ppm. With the transition to the ferricrete zone above the limonite zone, the Sc values decrease and present values between 1 ppm and 11.7 ppm. Therefore, the Sc content, which is 9.7 ppm on average in the protolith serpentinite at the bottom of the first profile of the Hematite pit, becomes approximately 3.5 times richer in the limonite zone with a progressive increase, reaching an average of 33.85 ppm. The highest Sc values of 63.6 ppm and 65.7 ppm are observed at the middle-upper level of the limonite zone and show ~6 times enrichment. Similarly, in the second lateritic weathering profile, scandium enriches progressively from the serpentinite protolith (10.83 ppm) towards the limonite zone (17.98 ppm). The maximum Sc concentration in this profile is 53.6 ppm, although it is detected in a sample at the middle-upper level of the limonite zone, indicating that the serpentinite is enriched by ~5 times.

Progressive enrichment of scandium from the bedrock serpentinite to the limonite zone in the Hematite Pit and a systematic decrease in the upper levels of the laterite are also observed in other lateritic Ni deposits with Sc enrichment and suggests that scandium, which is removed by the dissolution of serpentinite, is generally adsorbed on goethite (Chassé et al., 2017) and/or integrated into the crystal structure of goethite instead of Fe^{3+} (Munoz et al., 2017). However, the decrease in Sc values in the upper laterite zone is likely related to the progressive dissolution of goethite (e.g., Ulrich et al., 2019). Although at the upper laterite level, some scandium may be incorporated into the crystal structure of hematite (Chassé et al., 2017), the absence of hematite in the ferricrete zone in the Çaldağ deposit may indicate that the scandium mobilized from the dissolving goethite is removed from the system.

Chassé et al. (2017) states that during lateritic weathering, scandium behaves like rare earth elements due to its ionic radius and has an enrichment factor of 5, with an average of ~7-8 in scandium lateritic Ni deposits (Aiglsperger et al., 2016; Jaireth et al., 2014; Maulana et al., 2016; Ulrich et al., 2019), and may indicate maximum enrichment of 10 times. The enrichment factor of scandium calculated from the Hematite pit is ~5-6, although close to these values, the maximum Sc values obtained from the pit are between 53.6-65.7 ppm. These values are below the ~100 ppm Sc (Aiglsperger et al., 2016; Maulana et al., 2016; Chassé et al., 2017) that is the value required for potential of scandium to be exploited as a by-product in

lateritic Ni deposits. However, the Syerston-Flemington deposit in eastern Australia, where scandium is extracted as the main product, has 1350 tons of Sc reserve (Pursell, 2016) with an average Sc concentration of 434 ppm (Chassé et al., 2017) and the maximum enrichment factor in the deposit (parent rock ~80 ppm, limonite zone ~800 ppm) was calculated as ~10. Although the enrichment factor (~5-6) of scandium in the Çaldağ deposit is close to the average factor (~7-8) in similar deposits with Sc potential, the maximum Sc concentrations in the pit (53.6-65.7 ppm) are quite low in terms of the by-product potential of scandium in the deposit. The reason behind this is considered to be related to the content of the protolith (parent rock) serpentinized peridotite in the Çaldağ deposit and the tectonic stability of it. According to mineral chemistry studies, scandium is mostly found in pyroxene (~60 ppm) of ultramafic bedrock minerals, but contains much lower amounts of Sc (<5 ppm) in hornblende, olivine and biotite (Leeman and Scheidegger, 1977; Aiglsperger et al., 2016; Maulana et al., 2016; Ulrich et al., 2019). The average 9-10 ppm Sc values obtained from protolith serpentinite in the Çaldağ deposit can be explained by (1) the olivine minerals observed in the related bedrock peridotite (Thorne et al., 2009) and (2) the least serpentinized ultramafics as dunite and harzburgite (Helvacı et al., 2018). High enrichment of scandium in related deposits is associated with long-lasting weathering processes of the Sc-containing bedrock in a stable tectonic environment (Chassé et al. 2017). Accordingly, the fact that the Çaldağ deposit has been affected by extensional tectonic regime after the suggested main lateritization period (Middle Eocene; Thorne et al., 2009) since the latest Oligocene (e.g. Bozkurt, 2001; Gülyüz et al. 2024a) and has not been exposed to a stable weathering is thought to be another factor negatively affecting the scandium enrichment in the deposit.

South pit

The Sc concentration in the South pit profile shows a different distribution compared to that in the Hematite pit, although it does not show any regular trend. 11.2 ppm and 14.7 ppm Sc concentrations are obtained from the protolith, while lower Sc content is detected in the limonite zone at 2.8 ppm, 5.6 ppm, and 10.7 ppm values. The Sc contents of the bedrock in the pit (11.2 ppm and 14.7 ppm) are higher than the values in the bedrock of the hematite pit (7.6–12 ppm). The protolith of the relevant pit, the ultramafic bedrock cropping out around the pit, is defined as partially serpentinized pyroxenite (Helvacı et al., 2018), and it is thought that the Sc content is relatively high due to the pyroxene minerals it contains. Although the relatively high Sc content in the bedrock can cause Sc enrichment (~100 ppm) with the potential to be exploited in the limonite zone by lateritic weathering, it is dependent on the Eh-pH conditions associated with the secondary oxidation and alteration/weathering processes that the limonite zone is exposed to, such as faulting and transportation after lateritization in the South pit. It is hence suggested that although the limonite zone was enriched with Sc, Sc contents (2.8–10.7 ppm) may have decreased with the dissolution of Sc-containing minerals, most likely goethite. Similar to Sc, limonite zone has lower Ni contents compared to protolith, that is most likely related to the dissolution of goethite during post-lateritization deformation related secondary weathering and alteration processes.

CONCLUSIONS

This study investigates the distribution of scandium (Sc) in the unweathered parent rocks

and various laterite zones within two different pits of the Çaldağ lateritic Ni-Co deposit.

The initial Sc content of the unweathered parent rocks represents a crucial factor influencing the maximum Sc grades in their lateritized derivatives. The serpentinite protolith at the bottom of the lateritic profiles in the Hematite pit has an average Sc content of 10.3 ppm. Scandium shows a slight increase from the serpentinite protolith to the limonite and is significantly enriched in the middle-upper levels of the limonite zone, with elevated concentrations reaching up to ~66 ppm. This corresponds to a sixfold increase in Sc content compared to the serpentinite protolith. Although the enrichment factor (~5–6) of scandium in the Hematite pit is close to the average factor (~7–8) in similar deposits with Sc potential, the maximum Sc concentrations in the deposit (53.6–65.7 ppm) are comparatively low when contrasted with the by-product potential of scandium (~100 ppm) in nickel laterites. This is likely due to the low Sc content of the protolith in the pit and the lack of tectonic stability after the main lateritization period.

Overall, the lateritic profile in the South pit shows a different pattern from the profile in the Hematite pit. Although the protolith at the bottom of the South pit has higher Sc contents compared to the Hematite pit (~13 ppm), lower Sc contents, averaging ~6.4 ppm, are found in the limonite zone. Despite the high Sc enrichment potential of the protolith pyroxenite from lateritic weathering (Rangott et al., 2016), post-lateritization weathering/alteration events in the pit likely caused a decrease in Sc contents by dissolving potential Sc-hosting minerals in the limonite zone.

In conclusion, the limonite zones of laterites in the Çaldağ deposit exhibit Sc concentrations up to 66 ppm, indicating low potential for Sc as a by-product alongside Ni production. However, this finding is limited by the study of three lateritic profiles within the two pits of the deposit. Therefore, more detailed and comprehensive mineralogical and geochemical studies on the occurrence of Sc in the Çaldağ deposit as well as lateritic deposits with various unweathered parent rocks in Türkiye are necessary to better examine the mechanisms behind the presence of scandium within Turkish laterites.

ACKNOWLEDGEMENTS

This study was supported by the Scientific and Technological Research Council of Türkiye (Grant no: 120Y275). The Institute of Rock Structure and Mechanics of the Czech Academy of Sciences is acknowledged for providing research facilities and a supportive work environment, which significantly contributed to the successful completion of this study. Sincere thanks are extended to Çaldağ Nikel Mining Company and Derya Psav for their invaluable assistance with the fieldwork. I also express my gratitude to Editor-in-Chief Elif Varol-Muratçay and the two anonymous reviewers for their constructive comments, which greatly improved the quality of the paper.

REFERENCES

Ailsperger, T., Proenza, J.A., Lewis, J.F., Labrador, M., Svojtka, M., Rojas-Puron, A., Longo, F., and Durisova, J., 2016. Critical metals (REE, Sc, PGE) in Ni laterites from Cuba and Dominican Republic. Ore Geology Reviews, 73, 127-147. DOI: 10.1016/j.oregeorev.2015.10.010

Akdeniz, N., 1980. Başlamış Formasyonu. Jeoloji Mühendisliği, 10, 39–47.

Audet, M.-A., 2009. Le massif du Koniambo, Nouvelle-Calédonie: Formation et obduction d'un complexe ophiolitique du type SSZ: enrichissement en nickel, cobalt et scandium dans les profils résiduels. Université de la Nouvelle-Calédonie et

Université du Quebec, PhD Thesis, 336p, Quebec.

Bozkurt, E., 2001. Neotectonics of Turkey—a synthesis. Geodinamica Acta, 14, 3–30. DOI: 10.1080/09853111.2001.11432432

Bozkurt, E., and Sözbilir, H., 2004. Tectonic evolution of the Gediz Graben: field evidence for an episodic, two-stage extension in western Turkey. Geological Magazine, 141, 63–79. DOI: 10.1017/S0016756803008379

Brookins, D.G., 1988. Eh–pH Diagrams for Geochemistry. Springer-Verlag, 176p, Berlin.

Chassé, M., Griffin, W.L., Reilly, S.Y.O., and Calas, G., 2017. Scandium speciation in a world-class lateritic deposit. Geochemical Perspectives Letters, 3, 105-114. DOI: 10.7185/geochemlet.1711

Chassé, M., Griffin, W.L., O'reilly, S.Y., Calas, G., 2019. Australian laterites reveal mechanisms governing scandium dynamics in the critical zone. Geochimica et Cosmochimica Acta, 260, 292–310. DOI: 10.1016/j.gca.2019.06.036

Chassé, M., Blanchard, M., Cabaret, D., Juhin, A., Vantelon, D., Calas, G., 2020. First-principles modeling of X-ray absorption spectra enlightens the processes of scandium sequestration by iron oxides. American Mineralogist, 105 (7), 1099–1103. DOI: 10.2138/am-2020-7308

Çolakoğlu, A.R., 2009. Geochemical and mineralogical characteristics of Fe-Ni laterite ore of Sarıçimen (Çaldıran-Van) area in Eastern Anatolia, Turkey. Turkish Journal of Earth Sciences, 18(3), 449-464. DOI: 10.3906/yer-0803-5

Elitok, Ö., and Tavlan, M. 2019. Geology and Economic Potential of Ni Deposits. pp 639-653. Pirajno, F., Ünlü, T., Dönmez, C., Şahin, M.B., ed. 2019. Mineral Resources of Turkey, Springer, Switzerland, 749p.

Emsley, J., 2014. Unsporting scandium. Nature Chemistry, 6, 1025. DOI: 10.1038/nchem.2090

European Commission, 2017. Study on the review of the list of critical raw materials", "Report of the Ad hoc Working Group on Defining Critical Raw Materials. https://ec.europa.eu/docsroom/documents/25421/attachments/1/translations/en/renditions/native, 27.05.2024 (Access Date: 23.08.2024).

Fandeur, D., Juillot, F., Morin, G., Olivi, L., Cognigni, A., Ambrosi, J.-P., Guyot, F.O., and Fritsch, E., 2009. Synchrotron-based speciation of chromium in an Oxisol from New Caledonia: Importance of secondary Fe-oxyhydroxides. American Mineralogist, 94, 710. DOI: 10.2138/am.2009.3073

Gambogi, J., 2018. Scandium, U.S. Geological Survey, Mineral Commodity Summaries. 144-145. https://mineralsmakelife.org/wp-content/uploads/2018/06/Minerals_Commodities_Summaries_2018.pdf, 27.05.2024 (Access Date: (Access Date: 23.08.2024).

Gleeson, S.A., Butt, C.R.M., and Elias, M., 2003. Nickel laterites: a review. Society of Economic Geologists Newsletter, 54, 9–16. DOI: 10.5382/SEGnews.2003-54.fea

Gülyüz, N., Gülyüz, E., Karaoğlan, F., and Kuşcu, İ., 2024a. Low temperature thermochronology reveals tilting of crystalline bodies, Halilaga porphyry Cu-Au deposit, NW Anatolia: Implications for exploration of porphyry copper deposits and interpretation of low-temperature thermochronology data for regional tectonics. Ore Geology Reviews, 166, 105958. DOI: 10.1016/j.oregeorev.2024.105958

Gülyüz, N., Kuşcu, İ., Danišík, M., 2024b. Application of (U-Th)/He hematite geochronology to the Çaldağ lateritic Ni-Co deposit, Western Anatolia: Implications for multi-stage weathering events during interglacial periods/segments. Ore Geology Reviews, 172, 106203. DOI: 10.1016/j.oregeorev.2024.106203

Helvacı, C., Gündoğan, İ., Oyman, T., Sözbilir, H., and Parlak, O., 2013. Çaldağ (Turgutlu-Manisa) lateritik Ni-Co yatağının jeolojisi, mineralojisi ve jeokimyasal özellikleri. Yerbilimleri, 34(2), 101-132.

Helvacı, C., Kadir, S., Güven, N., Oyman, T., Gündoğan, İ., Sözbilir, H., and Parlak, O., 2018. Mineralogy and genesis of the Ni-Co lateritic regolith deposit of the Çaldağ area (Manisa, western Anatolia), Turkey. Canadian Journal of Earth Sciences, 55(3), 252-271. DOI: 10.1139/cjes-2017-0184

Jaireth, S., Hoatson, D.M., and Miezitis, Y., 2014. Geological setting and resources of the major rare-earth element deposits in Australia. Ore Geology Reviews, 62, 72-128. DOI: 10.1016/j.oregeorev.2014.02.008

Kaya, O., Ünay, E., Saraç, G., Eichhorn, S., Hassenruck, S., Knappe, A., Pekdeğer, A., and Mayda, S., 2004. Halitpaşa transpressive zone: Implications for an Early Pliocene compressional phase in central western Anatolia, Turkey. Turkish Journal of Earth Sciences, 13, 1–13.

Kılıç, S., Sayılı, İ.S., and Akıska, S. 2021. Mineralogical-petrographical indications on Eskişehir-Karaçam Lateritic Nickel-Iron Ore Deposit. 73rd Geological Congress of Turkey, 24-28 Mayıs, Ankara, Türkiye, 789-790.

Koçyiğit, A., Yusufoğlu, H., and Bozkurt, E., 1999. Evidence from the Gediz graben for episodic two-stage extension in western Turkey. Journal of the Geological Society, London, 156, 605–616. DOI: 10.1144/gsjgs.156.3.0605

Leeman, W.P., and Scheidegger, K.F., 1977. Olivine/liquid distribution coefficients and a test for crystal-liquid equilibrium. Earth and Planetary Science Letters, 35 (2), 247-257. DOI: 10.1016/0012-821X(77)90128-5

Lips, A.L.W., Cassard, D., Sözbilir, H., and Yılmaz, Y., 2001. Multistage exhumation of the Menderes Massif, western Anatolia (Turkey). International Journal of Earth Sciences, 89, 781–792. DOI: 10.1007/s005310000101

Marsh, E., Anderson, E., and Gray, F., 2013. Nickel-Cobalt laterites—a deposit model. U.S. Chapter H of Mineral deposit models for resource assessment. U.S. Geological Survey. DOI: 10.3133/sir20105070H

Maulana, A., Sanematsu, K., and Sakakibara, M., 2016. An overview on the possibility of scandium and REE occurrences in Sulawesi, Indonesia. Indonesian Journal on Geoscience, 3(2), 139-147. DOI: 10.17014/ijog.3.2.139-147

Muñoz, M., Ulrich, M., Levard, C., Rose, J., Ambrosi, J.-P., Cathelineau, M., Teitler, Y., Marcaillou, C., and Hesse, B., 2017. Distribution and speciation of Sc in lateritic profiles of New Caledonia using synchrotron-XRF and Sc K-edge XANES spectroscopy. International Workshop on the Geochemical Cycle of Ni, Co and Sc: from mining exploration to ecotoxicity, October 17-19, Nancy, France.

Okay, A.İ. and Siyako, M. 1993. The revised location of the İzmir-Ankara Suture in the region between Balıkesir and İzmir. Tectonics and Hydrocarbon Potential of Anatolia and Surrounding Regions, Ozan Sungurlu Symposium Proceedings. Association of Turkish Petroleum

Geologists, 1993, Ankara, Türkiye, 333-355.

Okay, A.İ., and Tüysüz, O. 1999. Tethyan sutures of northern Turkey. pp. 475-515. Durand, B., Jolivet, L., Horvath, F., Seranne, M., ed. 1999. The Mediterranean Basins: Tertiary Extension within the Alpine Orogen. The Geological Society London, Special Publications, London, UK. DOI: 10.1144/gsl.sp.1999.156.01.22

Okay, A.I., Satır., M., Maluski, H., Siyako, M., Monie, P., Metzger, R., and Akyüz, S., 1996. Paleo- and Neo-Tethyan events in northwestern Turkey: Geologic and geochronologic contraints. pp. 420-441. Yin, A., Harrison, T.M., ed. 1996. The Tectonic Evaluation of Asia. Cambridge University Press, Camridge, UK, 666p.

Oze, C., Fendorf, S., Bird, D.K., and Coleman, R.G., 2004. Chromium geochemistry of serpentine soils. International Geology Review, 46(2), 97-126. DOI: 10.2747/0020-6814.46.2.97

Önoğlu, N. 2000. Early Eocene nummulitides and alveolines of western Anatolia. 53rd Geological Congress of Turkey, 21-25 Şubat, Ankara, Türkiye, 270–272.

Polyak, D.E., 2018. Vanadium. U.S. Geological Survey, US.

Pursell, D.C., 2016. Quarterly Report. Jervois Mining Ltd, Cheltenham, Australia.

Qin, H.B., Yang, S., Tanaka, M., Sanematsu, K., Arcilla, C., Takahashi, Y., 2020. Chemical speciation of scandium and yttrium in laterites: New insights into the control of their partitioning behaviors. Chemical Geology, 552, 119771. DOI: 10.1016/j.chemgeo.2020.119771

Rangott, M., Hutchin, S., Basile, D., Ricketts, N., Duckworth, G., Rowles, T.D., 2016. Feasibility study - Nyngan Scandium Project Bogan Shire, NSW, Australia. NI 43-101 Technical Report by Scandium International Mining Corp.

Samson, I.M., Chassé, M. 2016. Scandium. pp. 1-4. White, W.M., ed. 2016 Encyclopedia of Geochemistry, Springer International Publishing, Cham, Switzerland. DOI: 10.1007/978-3-319-39193-9_281-1

Serin, B., 2020. Karaçam (Sivrihisar, Eskişehir) ve çevresindeki demir, nikel zenginleşmelerinin mineralojisi, petrografisi ve jeokimyası. Ankara Üniversitesi, Fen Bilimleri Enstitüsü, Jeoloji Mühendisliği Anabilim Dalı, Yüksek lisans Tezi, 43s, Ankara.

Tavlan, M., Thorne, R., and Herrington, R.J., 2011. Uplift and lateritization history of the Çaldağ ophiolite in the context of Neo-Tethyan ophiolite obduction and uplift: implications for the Cenozoic weathering history of western Anatolia. Journal of the Geological Society, 168, 927-940. DOI: 10.1144/0016-76492010-086

Teitler, Y., Cathelineau, M., Ulrich, M., Ambrosi, J.-P., Munoz, M., and Sevin, B., 2019. Petrology and geochemistry of scandium in New Caledonian Ni-Co laterites. Journal of Geochemical Exploration, 196, 131–155. DOI: doi.org/10.1016/j.gexplo.2018.10.009

Thorne, R.L., Herrrington, R., and Roberts, S., 2009. Composition and origin of the Çaldağ oxide nickel laterite, W. Turkey. Miner Deposita, 44, 581-595. DOI: 10.1007/s00126-009-0234-6

Thorne, R.L., Roberts, S., and Herrington, R., 2012. Climate change and the formation of nickel laterite deposits. Geology, 40(4), 331-334. DOI: 10.1130/G32549.1

Traore, D., Beauvais, A., Chabaux, F., Peiffert, C., Parisot, J., Ambrosi, J.-P., and Colin, F.,

2008. Chemical and physical transfers in an ultramafic rock weathering profile: part 1. Supergene dissolution of Pt-bearing chromites. American Mineralogist, 93, 22. DOI: 10.2138/am.2008.2605

Ulrich, M., Cathelineau, M., Munoz, M., Boiron, M-C., Teitler, Y., and Karpoff, A.M., 2019. The relative distribution of critical (Sc, REE) in some Ni-laterite deposits of New Caledonia. Journal of Geochemical Exploration, 197, 93-113. DOI: 10.1016/j.gexplo.2018.11.017

Wang, Z., Li, M.Y.H., Liu, Z.-R. R., Zhou, M.-F., 2021. Scandium: Ore deposits, the pivotal role of magmatic enrichment and future exploration. Ore Geology Reviews, 128, 103906. DOI: 10.1016/j.oregeorev.2020.103906